Soft Matter

Symmetry-derived Structure Directing Agents for Two-dimensional Crystals of Arbitrary Colloids

Journal:	*Soft Matter*
Manuscript ID	SM-ART-06-2021-000875.R1
Article Type:	Paper
Date Submitted by the Author:	03-Aug-2021
Complete List of Authors:	Mahynski, Nathan; National Institute of Standards and Technology, Chemical Sciences Division Shen, Vincent; National Institute of Standards and Technology

Soft Matter

ARTICLE TYPE

Cite this: DOI: 00.0000/xxxxxxxxxx

Symmetry-derived Structure Directing Agents for Two-dimensional Crystals of Arbitrary Colloids†

Nathan A. Mahynski,*[a] Vincent K. Shen,[a]

Received Date
Accepted Date

DOI: 00.0000/xxxxxxxxxx

We derive properties of self-assembling rings which can template the organization of an arbitrary colloid into any periodic symmetry in two Euclidean dimensions. By viewing this as a tiling problem, we illustrate how the shape and chemical patterning of these rings are derivable, and are explicitly reflected by the symmetry group's orbifold symbol. We performed molecular dynamics simulations to observe their self-assembly and found 5 different characteristics which could be easily rationalized on the basis of this symbol. These include systems which undergo chiral phase separation, are addressably complex, exhibit self-limiting growth into clusters, form ordered "rods" in only one-dimension akin to a smectic phase, and those from symmetry groups which are pluripotent and allow one to select rings which exhibit different behaviors. We discuss how the curvature of the ring's edges plays an integral role in achieving correct self-assembly, and illustrate how to obtain these shapes. This provides a method for patterning colloidal systems at interfaces without explicitly programming this information onto the colloid itself.

Colloidal materials are ubiquitous in nature and their technological importance in fields ranging from medicine to material science is now well-appreciated.[1–6] These materials tend to derive their utility from the arrangement of their constituents, intrinsically linking their structure to their function. Approaches to engineer the self-assembly of these systems into a specified arrangement generally involve tuning the geometry of the colloid itself, its surface functionalization, or use of an external field to direct the assembly.[2,7] Thus, synthetic control over the colloid is often required, making it challenging to assemble colloids whose physical nature may encode desirable properties, and are therefore immutable; for example, a monoclonal antibody or other functional molecule.

In three dimensions, DNA-based nanoscale frameworks have been designed to recruit colloids or other small molecules to organize their structure or enhance reaction pathways.[8] While the recruitment mechanism must be programmed, this is a general and powerful method for organizing components with relatively minimal modifications to the colloid itself;[9] however, to date only a limited number of crystallographic symmetries have been achieved with these frameworks.[10–12] DNA nanotechnology has also enabled the production of two dimensional (2D) self-assembling tiles which can be rationally designed based on tiling theory.[13–15] Here we demonstrate how principles of symmetry, related to isohedral tilings, can be used to derive structure directing agents (SDAs) that can, in principle, self-assemble into a planar framework with any desired 2D crystallographic symmetry, providing a template for an arbitrary colloid. These principles are not specific to any physical system and could be realized in different ways. Such patterned, functional interfaces play a key role in molecular recognition processes in immunological assays,[16–19] chemical separations,[3,20–23] cellular membranes,[24] and catalysis.[3,25,26] They are also important for creating advanced metamaterials and structural color.[3,27,28]

Properties of planar tilings and their connection to symmetry have been known in the field of mathematics for some time.[29] Thurston's concept of using orbifolds to study such geometrical groups[30] and Conway's subsequent naming convention have been studied for more than 30 years.[31] This topological approach to describing symmetry is unconventional, even in crystallography, though its elegance has elicited recent advocacy for its wider adoption.[32] In our view, this topological way of thinking provides an intuitive, yet underutilized paradigm for the programmable self-assembly of soft matter systems.

The SDA must be a topological ring to encircle the colloid being organized in a stereospecific manner, and we assume that its shape and chemistry will be fixed [*cf.* Fig. 1(a)]. It could also be a filled disc if the colloid is tethered above the plane of SDA's surface rather than being enclosed by it. If we consider this SDA-colloid pair to be a "tile", then we are simply seeking all possible tiles that self-assemble into different symmetries. By viewing this as a tiling problem we exploit the fact that these properties are

[a] *Chemical Sciences Division, National Institute of Standards and Technology, Gaithersburg, Maryland 20899-8320, USA. Tel: +1 301-975-6836; E-mail: nathan.mahynski@nist.gov*

† Electronic Supplementary Information (ESI) available: derivation of SDA shape and sequence from symmetry diagrams, simulation details, and full simulation results. See DOI: 10.1039/cXsm00000x/

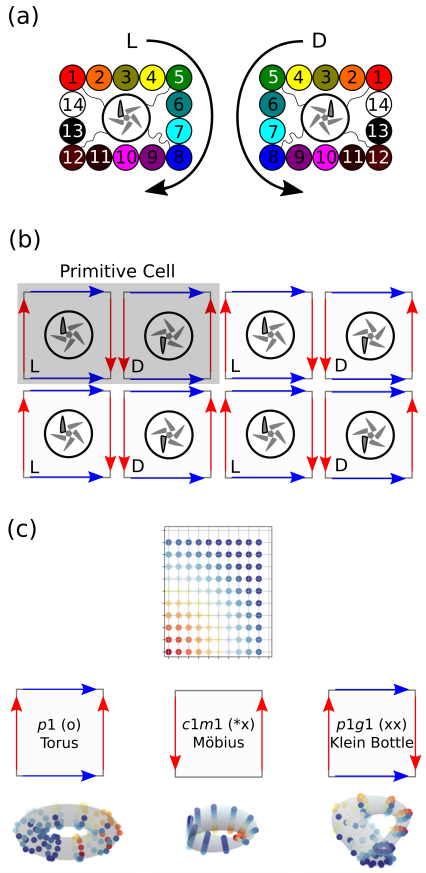

Fig. 1 Description of a colloidal structure direction agent (SDA) and orbifolds. (a) Depiction of the polymer SDA as a ring (or disc) which tethers the colloid to be organized. The identities, indicated by color, of each enumerated location are given in a left-handed (L) fashion and for its enantiomorph (D). (b) A $p1g1$ (××) crystal is created by combining two fundamental domains of opposite chirality to form a primitive cell, which can create the crystal by translation operations alone. Symmetrically equivalent edges are indicated by colored arrows. (c) Fundamental domains showing edge pairing for 3 different plane symmetry groups; edges with the same colored arrows should be wrapped to match the direction of their arrows, resulting in their orbifold.

derivable from symmetry and that there exist a finite number of possible tiles.[29]

Consideration is given to the fact that experimental synthesis of such structures is likely to occur in 3D, followed by some form of deposition to an interface; this practically impacts the ability to control the chirality of the mixture, which is a factor in our design. We derive example SDAs that assemble into each wallpaper group, and discuss the necessity of curvature along the SDA's edges to correctly encode symmetry in our model; we further elucidate the role of a ring's chirality and organize the wallpaper groups according to characteristics of their self-assembly, which can be rationalized on the basis of their orbifold symbol.

This manuscript is organized as follows. In Sec. 1 we review relevant concepts of symmetry and illustrate how to obtain an SDA for each plane symmetry group. We discuss simulation details in Sec. 2, then present our organization of these groups in Sec. 3. This is followed by a discussion of potential routes to experimental realization in Sec. 4, and a summary of our conclusions in Sec. 5.

1 Background

There are 17 plane symmetry, or wallpaper, groups that describe all unique combinations of isometries that properly tessellate the 2D Euclidean plane when operating on a unit of space referred to as the fundamental domain (FD) or "asymmetric unit." The FD is essentially a topological disc whose boundary is decorated with the group's symmetry operators. The FD has two properties that are important in the context of this work. First, it is the smallest possible simply connected area that covers the plane by group operations making it the natural "atomic unit" of the crystal. Second, it encloses no symmetry elements that belong to the wallpaper group, hence the "asymmetric" moniker.[33] The latter property implies that any asymmetric object may be placed within it without disrupting the symmetry of the crystal. Importantly, this implies that the design is valid for any asymmetric colloid if we base the SDA on a crystal's FD. This is usually also valid for colloids which have some degree of point-preserving symmetry (such as rotational) as well, though under special conditions where a colloid has a certain set of symmetries and is placed in a precise location and orientation, it may increase the global symmetry of the pattern. This is addressed in Sec. 4, but we regard this as an exception to the general case. Thus, we treat the SDA as a tile which corresponds to the FD of a desired wallpaper group. The tile's boundary is regarded as a ring discretized into beads, enclosing the colloid. The identity of these beads and shape they form are what we seek [*cf.* Fig. 1(a)].

1.1 Symmetry defines chemical identities

There are four isometries of the plane including translation, rotation, reflection, and glide reflection. Numerous mathematical descriptions and conventions describing how groups of these operations generate patterns have been developed, but are almost exclusively based on specifying a pattern's generators.[34] Philosophically, these focus on the "interior" of the FD and how that pattern is systematically repeated by a group *via* matrix operations, for example. An alternative description based on topology uses the concept of orbifolds (orbit manifolds),[30,32,34–36] and instead is a more explicit description of the domain's boundary.

Since the FD is a tile that tessellates the plane, each of it's edges will coincide with an edge of a neighboring image, implying they are symmetrically equivalent. For example, the edges denoted with blue arrows in Fig. 1(b) are the result of translations, red arrows correspond a glide operation. The orbifold may be constructed by taking a single FD and folding it to superimpose, or "glue" together,[32] equivalent positions, as shown in Fig. 1(c). More detailed descriptions of these orbifolds and their connection to crystallographic groups may be found in Refs.[30,32,34,36,37] and elsewhere. In essence, this is a topological description of symmetry as a surface that relies on how the perimeter of the FD is related to itself by symmetry, akin to adjacency diagrams and incidence symbols often used to describe tilings.[29,38] Importantly, each wallpaper group is described by a single, unique orb-

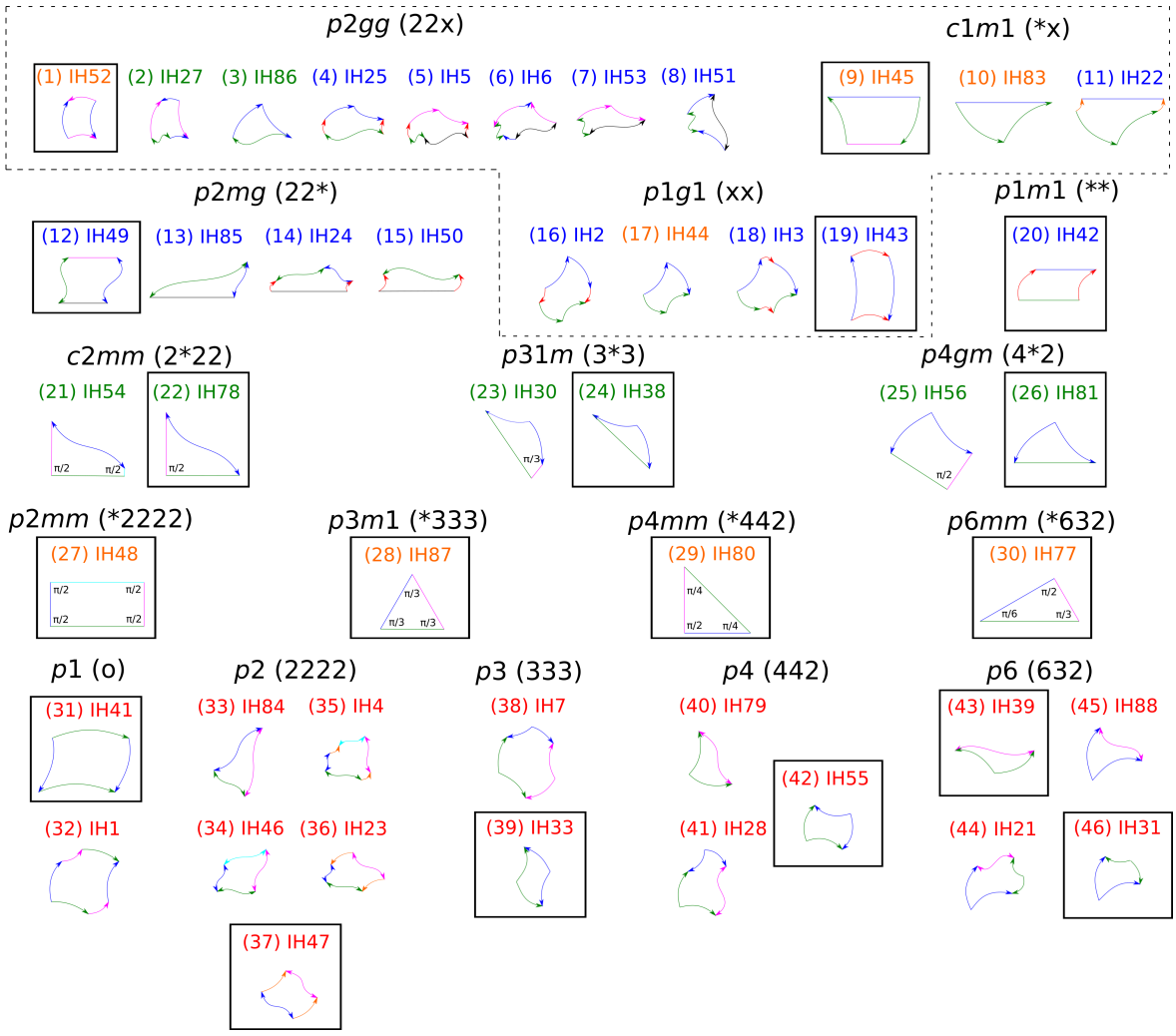

Fig. 2 The 46 possible isohedral (IH) tiles corresponding to a FD for each wallpaper group, given here by its international name followed in parentheses by its orbifold symbol. The number in parentheses is specific to this work, whereas the IH designation corresponds to Ref. [29]. Similarly colored edges are symmetrically equivalent in the direction of their arrows. Edges which can be deformed, as described in Fig. 3, are the result of symmetry operations and equivalent edges from pairs of tiles must have their concavities matched, as illustrated. Straight edges without arrowheads indicate a mirror and the angle between intersecting mirrors is explicitly shown; other fixed angles and constraints may be found in Ref. [29]. Tiles shown in black boxes were used in this work. Names are colored according to the self-assembly behavior described by Fig. 5: red, orange, green, and blue correspond to rows 5 through 2, respectively.

ifold.[34,39]

If we adopt the FD as our SDA, then the chemical identity of each point on the boundary is given by the pattern of symmetrically equivalent sites. This assumes that points with the same identity will interact favorably, while points that are different will not. In colloidal systems, these specific interactions are commonly encoded using DNA-based interactions, but may have other realizations as well.

1.2 Correct self-assembly requires curved edges

Since an orbifold represents a FD that has been glued together, it is possible to reverse the process and cut open the orbifold to recover the FD. However, for many wallpaper groups this cutting can occur in several different ways, resulting in different valid FDs.[34] These isohedral tiles have been enumerated previously,[29] but are perhaps most intuitively viewed as an exhaustive list of all possible graphs (cuts) on a given orbifold that produce an asymmetric unit.[34] There are 46 such tiles that correspond to FDs for the wallpaper groups, reproduced in Fig. 2.[29,34,40] Tiles differ by the number of edges (different colors) and the nature (*e.g.* translation or glide reflection) of their relationship to other edges. In the scope of this work, this is important because these properties of the tile will influence the self-assembly characteristics.

The simplest cutting operation would be to slice the orbifold in straight lines resulting in a polygonal FD. In general, however, a system of such polygons will not self-assemble into the correct symmetry. While it is possible for an external agent, á la Maxwell's demon, to assemble such polygons in a correct tessellation using *a priori* knowledge of the relative orientation and chirality of each tile, unguided assembly will generally fail because the chemical sequence along straight edges cannot unambiguously encode the symmetry operation that defines its match.

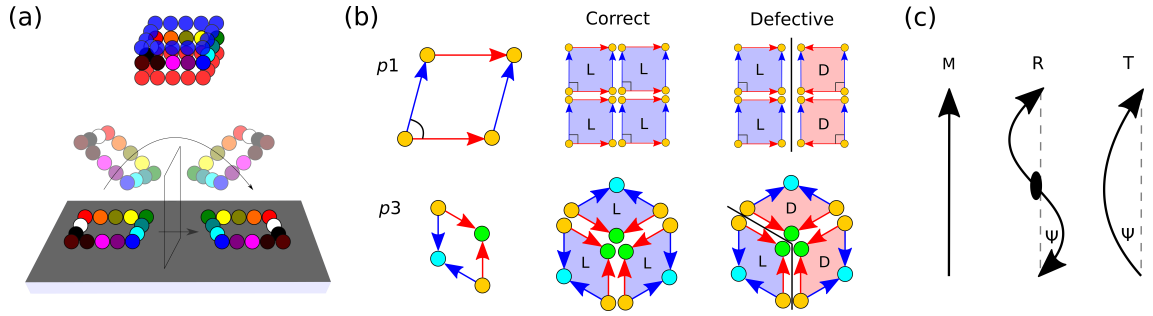

Fig. 3 The problem with using polygons as SDAs. (a) A ring rotated out of plane generates its chiral enantiomorph in plane, thus both enantiomorphs are expected to be present in practice. The 3-layered ring is used in this work to track chirality. (b) Fundamental polygons based on the FDs of p1 and p3. Identically colored edges and corners indicate symmetric equivalence. The correct self-assembly is the aggregation of polygons of the same chirality (here, L); however, examples that can form in a racemic mixture are shown with penalty-free defects that do not disrupt the growth of the aggregate. For this p1 example, the defect leads to p1m1 symmetry instead. For visual clarity, we have colored the tiles according to their "top layer." (c) The deformations applied to a fundamental polygon's edges that penalize defective assemblies: M for mirrored edges (no deformation), R for edges with a 2-fold rotation center, T for all others.

True "self"-assembly requires additional information. To see this, consider that it is possible to take any convex polygon and rotate it 180° out of plane using any chosen edge as the rotation axis [*cf.* Fig. 3(a)]. The edge used as this axis will match perfectly with its neighbor, which is now equivalent to a reflection of the original tile (its chiral enantiomorph). Thus, a straight edge could always match pairs of enantiomorphs regardless of what operation, such as a rotation or glide reflection, was supposed to occur to match a pair of tiles at that edge. As illustrated in panel (b), it is possible to repeat defects causing them to cancel out so their presence does not necessarily impede self-assembly; moreover, these orientationally disordered polymorphs have an identical energy to their correctly ordered counterpart since all edges end up matched, but will be favored by combinatorial entropy at finite temperature. This precludes correct self-assembly programmed by sequence alone in conventional 3D environments where rotational diffusion can occur.

An out-of-plane rotation as described is identical to an in-plane reflection [*cf.* Fig. 3(a)], neglecting anything out of plane (red and blue beads), meaning that if such a rotation is allowed then a racemic system is inevitable. We anticipate that, in practice, controlling the chirality of a mixture of rings at an interface will be difficult due to their rotational diffusion leading up to, or following, deposition to an interface. Deposition into 2D may fix the chirality of each ring, but will do so randomly (50% chance of L *vs.* D). Moreover, in some cases the SDA also may rotate after deposition; for example, if the assembly plane is a liquid-liquid interface which does not irreversibly pin the SDA.

To resolve this, one can deform the edge so it has non-zero local curvature, κ, along its arc as in Fig. 3(c). The simplest approach is to use a constant value, equivalent to a circle of radius, r, impacting the edge where $\kappa = 1/r$. Duplicating the curvature on a tile's matching edges means that when 2 tiles approach each other, correct alignments "nest" inside each other since they will have complementary curvatures, while incorrect alignments bend away from each other creating an energetic penalty by preventing points from matching up. Note that mirrored edges must remain straight. Here, we employ the simplest possible perturbation away from $\kappa = 0$, though in principle this remains a flexible design variable which need not be constant, nor the same along symmetrically distinct edges.

1.3 Orbifold naming conventions

While more details are available elsewhere,[30,32,34,36,37] here we briefly summarize Conway's naming convention for orbifolds and their meaning. This should make the organization proposed later transparent. A generic orbifold can be obtained by performing surgery on a sphere to introduce boundaries (mirrors), handles (translations), crosscaps (glides), and cones (rotations) which encode different symmetry operations and whose presence changes the Euler characteristic of the sphere's surface. By convention an orbifold's symbol is listed as $\circ^{\alpha}\mathrm{ABC}\cdots*\mathrm{abc}*\mathrm{def}\cdots\times^{\beta}$. This indicates the presence of different symmetry operators. Specifically, $\circ^{\alpha}$ indicates α topological handles ($\circ$). Capitalized letters preceding an asterisk, such as A, denote an A-fold rotation center. Lowercase letters following an asterisk denote a intersecting mirrors which result in an interior angle of π/a between neighboring mirrors. Finally, $\times^{\beta}$ denote the presence of β crosscaps ($\times$).[34,39] The Gauss-Bonnet theorem can be used to show that there are exactly 17 different orbifolds with an Euler characteristic of 0 which correspond exactly to the "glued together" FDs of different wallpaper groups.

1.4 Summary of Symmetry-derived SDAs

In summary, if we choose our self-assembling SDA to be the FD of a wallpaper group, we may use it to template the assembly of an arbitrary object. Moreover, the SDA's shape and chemical pattern are defined by our choice of tile, which both derive from the orbifold (by "cutting" it open) of a given group. In most cases, the choice of tile in Fig. 2 does not affect the self-assembly characteristics we categorize in this work. Tile geometry and edge relationships may be found in reference tables such as in Ref.[29]; however, these become more intuitive when the FD is placed on a conventional symmetry diagram as in Ref.[33]. To illustrate this, we have placed the tile we chose to simulate for each group on its symmetry diagram to provide a graphical derivation of the shape

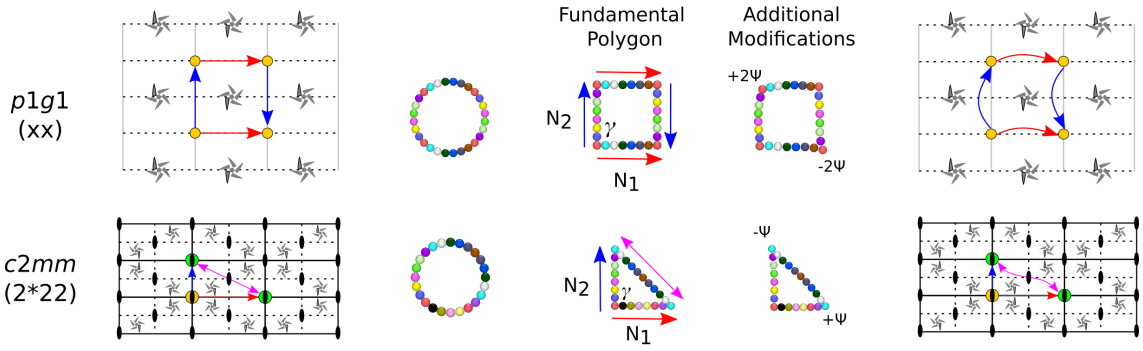

Fig. 4 Example derivation of SDA ring sequence and shape from symmetry diagrams presented in the International Tables for Crystallography, and how edge deformation is consistent with symmetry. A derivation for all wallpaper groups is available in the ESI.†

and relationship between the tile's edges. In Fig. 4 we illustrate this for 2 wallpaper groups, while the remaining groups are presented in the ESI.†

Consider the $p1g1$ group whose orbifold is a Klein bottle as in Fig. 1(c).[37] Choosing the fundamental domain as shown in Fig. 4, we have 2 pairs of edges (blue and red) which are symmetrically equivalent in the direction indicated by the arrows. Moving clockwise from the top left corner, we assign new identities to each discrete point (bead) until reaching the bottom right, except at the corner (which are all equivalent). Now symmetry starts to repeat the identities as shown by the color of each bead. Topologically, one can envision this as a labelled ring, as shown in Fig. 4. The fundamental polygon shows this encoding with colored arrows, and illustrates that we are free to choose any number of beads along adjacent edges (N_1 and N_2) and that $\gamma = \pi/2$. The edge deformations result in a change in the angle of $\pm 2\psi$ at opposite corners. Note that we are free to reverse the concavity of the red or blue (or both) curved lines; this simply changes which pair of corners the angle modification occurs at (as in examples 1 vs. 2 for $p6$ in the ESI†).

Next, consider the $c2mm$ group which has an orbifold designation of 2*22. The symbol indicates the presence of two mirror plane intersections forming angles of $\pi/2$, and a separate 2-fold rotation center. The bold lines in Fig. 4 trace out the mirror lines, which must form a rectangle to satisfy these requirements; the 2-fold rotation center exists in the center of this rectangle by necessity. This implies that only half of the rectangle formed by the mirror lines is the FD, since the other half is a rotated image of it. How the division occurs is unspecified and could take the form of a quadrilateral (IH54), for example, or the triangle (IH78) we have selected (*cf.* Fig. 2). The mirror lines (red and blue edges) imply they are not mapped to any other point on the FD, while the rotation center requires the contours of its edge to be symmetric about that center (magenta line). Thus, the FD must have $\gamma = \pi/2$, but N_1 and N_2 are free variables.

2 Methods

2.1 Model

Following previous work, we selected the shapes (tiles) for each group's FD used in Refs.[41] and[42]. In practice, depending on the system being used, it may be more reasonable to select one tile over the other, so several different possibilities have been explicitly simulated for $p6$ to illustrate this.

Each SDA ring was composed of 3 layers [*cf.* Fig. 3(a)], each made of a set of spherical beads with diameter σ bonded to its 2 nearest "lateral" neighbors, as well as its "vertical" neighbor(s) in adjacent layers. The upper and lower layers were purely repulsive with all other components, while the middle layer contained beads whose sequence (identities) was determined by symmetry. All beads in the model interacted through a truncated Lennard-Jones-like interaction.

$$U_{\text{pair}}(r) = \begin{cases} 4\varepsilon\left[\left(\frac{\sigma}{r}\right)^{2n} - \left(\frac{\sigma}{r}\right)^{n}\right] & r < r_{\text{cut}} \\ 0 & r \geq r_{\text{cut}} \end{cases} \quad (1)$$

Favorably interacting beads (beads of the same type) had their interaction truncated well past the minimum in energy ($|U_{\text{pair}}(r > r_{\text{cut}})| < 10^{-3}\varepsilon$, so $r_{\text{cut}} \approx 2.5\sigma$), while repulsive (beads of different types) had their interaction truncated at the minimum ($r_{\text{cut}} = 2^{1/n}\sigma$). In this work, we chose $\varepsilon = \sigma = 1.0$, which set the units of energy and length, respectively, by which all units are non-dimensionalized. We also selected $n = 9$ to make the interaction more close-ranged than its more common $n = 6$ counterpart.

The three layers were bound together by simple harmonic bonds between each bead in the middle layer and the bead above it (upper layer) and below it (lower layer), given by:

$$U_{\text{bond}}^{\text{inter}}(r) = k_{\text{b}}(r - \sigma)^2. \quad (2)$$

We set $k_{\text{b}} = 300\ \varepsilon/\sigma^2$. Bonds between neighbors within a layer were modeled as being "string-like" such that there was little to no energy penalty for fluctuating within set stretching limits, but quickly diverged beyond them. Such a potential was constructed by summing three contributions: two hyperbolic tangent functions to create a well, and an even degree polynomial, as in Eq. 3 (*cf.* ESI Fig. S8 for illustration†):

$$U_{\text{bond}}^{\text{intra}}(r) = \overbrace{\frac{\varepsilon}{2}\left[\tanh\left(\frac{r-r_0-w/2}{s}\right)-\tanh\left(\frac{r-r_0+w/2}{s}\right)\right]}^{(1)} + \overbrace{\varepsilon\left(\frac{r-r_0}{w/2}\right)^{2n}}^{(2)} \tag{3}$$

The width of the bond, w, varies from a minimum of $r=\sigma$ to a maximum of $r=F\sigma$, where F is the bond stretching factor. A buffer, $b=\sigma/5$ was added such that $w=\sigma(F-1)+b$. The bond's midpoint corresponds to $r_0=\sigma(F+1)/2$. Finally, we set $s=0.05$ and $n=9$.

The bond stretching factor along an edge is $F=1$ when an edge is not deformed (mirror), but if $\psi>0$, the lateral bonds between neighbors must increase to accommodate this. In can be shown that for an edge of length, L, with N beads placed along it (*cf.* ESI for derivation†):

$$F\sigma = 2\psi\left[\frac{\sin(\pi/2-\psi)}{\sin(2\psi)}\right]\left(\frac{L}{N-1}\right). \tag{4}$$

Equilibrium (target) angles, ϕ_0, at different corners are determined by the choice of a fundamental domain's geometry and by ψ. In this work we employed a harmonic form to describe the angle potential:

$$U_{\text{angle}}^{\text{inter}}(r) = k_{\text{a}}(\phi-\phi_0)^2, \tag{5}$$

where we set $k_{\text{a}}=300\ \varepsilon/\text{radians}^2$. Along an edge instead of a corner, ψ sets the equilibrium bond angle in the following way. Once N is chosen, each can be thought of as a vertex on a regular polygon containing M total vertices (*cf.* ESI Fig. S7 for illustration†).

$$M = \left\lceil\frac{N-1}{\psi/\pi}\right\rceil, \tag{6}$$

The interior angle of a regular M-gon follows as $\phi_0=\frac{\pi(M-2)}{M}$. Since we employed a single value of ψ for all edges of a chosen FD, edges with a different N will have a different ϕ_0 values. Of course, when there is no deformation, $\lim_{\psi\to 0}\phi_0=\pi$.

2.2 Scoring the Assembly

To score how correctly a system self-assembled, we examined all interacting pairs of rings. A ring was considered to interact with a neighbor across the edge that contained the most beads below a fixed cutoff distance, $r_{\text{c}}=1.5\sigma$. The side a corner bead belongs to is ambiguous so these were not counted, consistent with the choice to leave their interactions purely repulsive, as described in Sec. 2.3.

Some ring "A" that interacts with another ring "B" across a certain edge of A determines the expected orientation of each of the vectors along the edges of B. We define an expected angle, $\theta_i(j)$, that the vector along edge i on ring A should be rotated counterclockwise so that it matches its orientation on ring B, when B is correctly oriented across edge j of ring A. Even if ring B is placed incorrectly, it is possible that some its edges still point in the correct direction. As a result, we define the mean score as:

$$s_{A,B} = \frac{1}{N_{\text{e}}}\sum_j \cos\left[\theta_i(j)-\theta_i^{\text{ideal}}(j)\right], \tag{7}$$

where N_{e} is the number of edges on the FD (3 or 4 in this work). Importantly, the edge i is defined with respect to ring A; therefore, the expectation angle depends on which ring we examine the pair from. To make the score independent of which ring's perspective is taken, we define:

$$S_{A,B} = \frac{s_{A,B}+s_{B,A}}{2}. \tag{8}$$

Note that $-1\le S_{A,B}\le+1$, where $S_{A,B}=-1$ reflects a configuration where all the edges on an SDA are oriented the opposite direction they should be, while a value of $S_{A,B}=+1$ implies the opposite. Practically, it is important to recognize that $S_{A,B}<+1$ simply implies that an SDA is misaligned, though we caution that the significance of its value otherwise can be dependent upon both the group and the FD chosen. We can then define a global score for a system based on these pairwise interactions:

$$S = \langle N_{\text{n}}\rangle\langle S_{A,B}\rangle, \tag{9}$$

where $\langle N_{\text{n}}\rangle$ is the average number of interacting neighbors a ring has, and $\langle S_{A,B}\rangle$ is the average score of interacting pairs of rings. The ESI contains more details pertaining to this calculation.†

2.3 Simulations

Canonical molecular dynamics (MD) simulations were carried out using the LAMMPS package[43] available at http://lammps.sandia.gov. The system's equations of motion were only integrated in the x-y plane, while the z-direction was ignored to enforce a 2D simulation. This fixes the chirality of each ring for the duration of the simulation. Rings were initialized far apart in a large simulation box so as to be non-interacting, then their energy (from angles and bonds) was minimized to form their FD's shape. Next, the system was compressed to its target area, then allowed to relax for 10^6 time steps to produce an initial configuration at a reduced temperature, $T^*=k_{\text{B}}T/\varepsilon=1.5$, where k_{B} is Boltzmann's constant. Interactions were then switched on between beads of the same type. Beads located at the corner of a FD were left "inactive" (purely repulsive); this makes identifying edges which are interacting unambiguous, which is necessary when computing their assembly score.

The system was cooled to a final target temperature using a Nosé-Hoover thermostat with 5 thermostats in a chain, a damping constant of $T_{\text{damp}}=100$, and a timestep of $\delta t=0.0005\ \sigma(\varepsilon m)^{-1/2}$, where $m=1$ was used as the mass of a bead. This cooling typically occurred over the course of 10^7 steps; cooling as slowly as over 4×10^7 was also investigated and found to have no significant effect on the final structure. The simulation was then run for 2×10^8 steps over which 1000 snapshots were collected for analysis. Beads that were directly bonded, and those that were separated by 2 bonds had their pairwise interactions deactivated ("Dreiding" setting in LAMMPS). Beads adjacent to a FD's

corner may, in certain cases be forced to overlap if the angle is too acute, so this deactivation allows this if necessary. Unless otherwise stated, we examined $N_{\rm tot} = 50$ rings at $T^* = 0.35$ with $N = N_1 = N_2 = 8$ and $\gamma = \pi/2$ (when variable, *cf.* Fig. 4). Finally, we generally simulated systems at a surface coverage fraction, $f = 0.33$. We estimated this as:

$$f = \frac{N_{\rm tot} A_{\rm ring}}{A}, \tag{10}$$

where A was the total area of the two dimensional simulation cell, and $A_{\rm ring}$ was the estimated surface area of a ring. Section S3.2 in the ESI details how this was estimated for different rings.†

3 Results

We simulated the self-assembly of SDAs based on a FD selected for each wallpaper group under three different conditions: (a) a single-enantiomorph system with straight edges, (b) a racemic mixture with straight edges and, (c) a racemic mixture with deformed edges. We found that the resulting self-assembly characteristics could be broadly classified into 5 categories, given by different rows in Fig. 5. This organization of groups follows clear trends in the orbifold symbol, less evident by other naming conventions. Note that rows 1 and 4 contain descriptions of self-assembly characterized as "None". This corresponds to the case where at the low, but finite temperatures used in this work, the systems do not assemble; instead they behave like purely repulsive particles. The reason is that it is not possible to find alignment of more than a single bead at a time along any edge for the cases indicated. Examples are shown in Fig. 5. Strictly speaking, as $T^* \to 0$ we expect these systems to condense forming disordered solids, but at finite T^* the energetic driving force for aggregation is overwhelmed by configurational disorder driven by entropy. We use the term "None" as shorthand for this. Figure 6 illustrates representative results characterizing each row; results for all groups are available in the ESI.†

3.1 Row 5: Gyrations (Palindromes)

At the base of the pyramid is row 5. Figure 6 displays representative results taken from $p3$. If the system of SDAs is prepared as polygons with straight edges, it assembles essentially without defect when only a single chirality is allowed. The blue curves in Fig. 6 for $p3$ illustrates that whenever SDAs approach each other, they quickly orient themselves correctly ($\langle S_{\rm A,B}\rangle \to 1$) and are able to grow unimpeded as $\langle N_{\rm n}\rangle$ rises quickly, before slowly annealing into a single aggregate; we label this "2D, Ideal" assembly in Fig. 5. If the other enantiomorph is introduced (orange curves), each SDA finds essentially the same number of neighbors, while the quality of each interaction drops significantly ($\langle S_{\rm A,B}\rangle << 1$). We characterize this assembly as "2D, Defects."

This is a consequence of the fact that all wallpaper groups in row 5 are composed exclusively of rotation symmetries (gyrations). Indeed, the orbifold symbol includes only capitalized letters, *e.g.*, ABC; the exception to this is $p1$ (o), which is a result of no gyrations, nor any other symmetries except translation. Regardless, its self-assembly character is similar. Gyrations correspond to rotation of an edge about a corner; thus, the sequence of identities is locally repeated about that corner (center of rotation), but in the opposite order, *i.e.*, it is palindromic (*cf.* the magenta hypotenuse of $c2mm$ in Fig. 4, or the example of $p3$ given in Fig. 6). Palindromes in a single enantiomorph mixture assemble easily as one SDA simply rotates to align its corresponding edge with a neighbor; however, a polygonal SDA of the opposite chirality can easily do the same without interrupting the growth of the aggregate, as illustrated in Fig. 3(b).

As previously explained, this can be remedied by curving the edges, which causes matching edges on SDAs of opposite enantiomorphs to curve away from each other; only matching edges of SDAs of the same chirality can "interlock." As a result, all *L* enantiomorphs can easily assemble with each other, as can *D* enantiomorphs, while *L*-*D* interactions are penalized. Thus, a mixture of *L* and *D* enantiomorphs will phase separate into *L*-enriched and *D*-enriched domains. The snapshot in Fig. 6 shows a larger system ($N_{\rm tot} = 200$ rings) than in other cases ($N_{\rm tot} = 50$), to better illustrate this. The two phases form an interface, resulting from single bead or partial alignment as described in Fig. 5, which reduces $\langle S_{\rm A,B}\rangle$ slightly relative to the enantiomorphically pure case. The number of neighbors a system can form is unaffected, leading to a global score, S, which anneals to essentially the same level as in the "ideal," single enantiomorph case. Consequently, using curved edges allows a racemic SDA mixture to assemble correctly, albeit into phase separated domains. Tiles which behave like this are given in red in Fig. 2.

3.2 Row 4: Kaleidoscopes (Addressable Complexity)

Row 4 in Fig. 5 contains kaleidoscope groups composed exclusively of intersecting mirrors. A more precise topological description is that their orbifolds are exclusively composed of boundaries with corner points, as two non-intersecting mirrors can also be considered kaleidoscopic.[34] The orbifold symbols reflect this with numbers preceded by an asterisk, *e.g.*, *abc. As a result, the FDs are composed exclusively of straight edges and, with the exception of $p2mm$, have a uniquely defined shape. The FD for $p2mm$ (*2222) may be any rectangle since it is topologically formed by 4 right angles leaving the relative length of its sides unconstrained; however, the other groups in this row are triangles. For example, the symbol for $p3m1$ (*333) indicates 3 intersecting mirror lines which all form angles of $\pi/3$; this is the definition of an equilateral triangle and so there is no other possible shape. The orbifolds in these cases are simply the polygons given in Fig. 2.

Each FD for these kaleidoscopes is, by definition, completely surrounded by the enantiomorph of opposite chirality. Therefore, if only one enantiomorph is present it is not possible for an SDA to find a matching neighbor for any of its edges, suppressing aggregation by making all SDAs effectively purely repulsive toward one another. This is why Fig. 5 indicates there is no assembly in this case. Conversely, when the mixture is racemic, assembly proceeds perfectly, as shown in Fig. 6. Tiles exhibiting such behavior are shown in orange in Fig. 2.

A mirror implies that the symmetrically equivalent site for each point along an edge is itself; there exists no "mapping" to an equivalent location somewhere else on the FD's edges. Con-

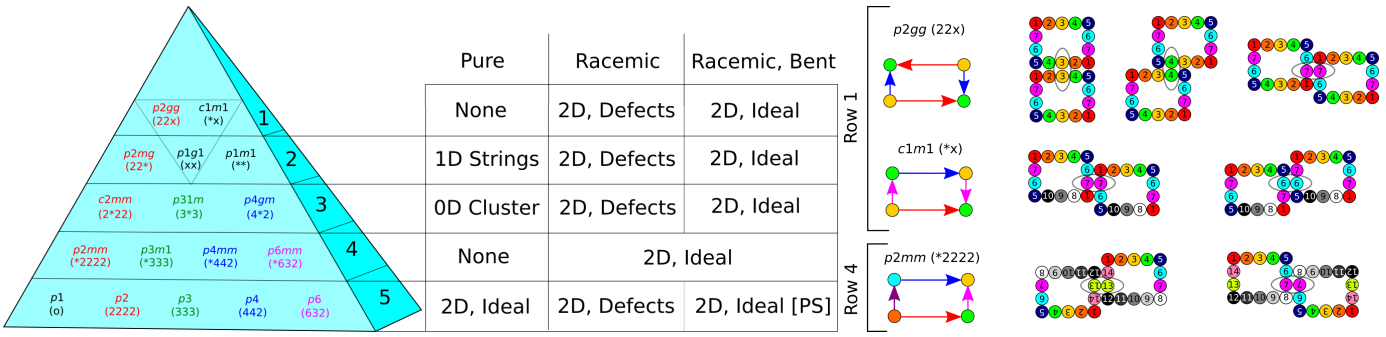

Fig. 5 Organization of the wallpaper groups by self-assembly characteristics. Here, similar groups are organized into rows, which are colored from left to right according to the highest rotational order present. The international name for each group is given with the orbifold symbol underneath in parentheses. Assembly characterized by "None" is graphically illustrated at the right, and discussed in the text; the bracket term "PS" refers to "phase-separated" in row 5. It is not possible to bend the edges of groups from row 4 so the "Racemic" columns are combined.

sequently, each point along the mirror is unique. If all edges are mirrors, the SDA's perimeter is composed entirely of unique points, making it addressably complex.[44,45] Since addressable complexity effectively programs the assembly to proceed in only one way, perfect assembly is observed. This approach has been leveraged to induce self-assembly of many carefully engineered structures.[9,46–50]

3.3 Row 3: Gyroscopes (Self-limiting clusters)

Row 3 contains "gyroscopic" groups which are hybrids of gyrations and kaleidoscopes.[34] For such groups, the orbifold symbol follows a pattern A*bc, for example, indicating an A-fold rotation center in the middle of a polygon created by intersecting mirrors (straight edges) forming angles of π/b and π/c. The leading capital letter in the orbifold symbol, A, indicates how many times this polygon is evenly divided. For example, with $c2mm$ (2*22), the outer boundary is a rectangle which is divided in half by any line which transects its center [*cf.* magenta curve in Fig. 4(a)]; here, we have elected to "cut" along the diagonal to create a triangular FD.

Mixtures containing FDs of only a single enantiomorph can assemble perfectly about the rotation center, as in row 5, to create 0D (point) clusters. After matching their rotated edges to create such a cluster, the resulting perimeter is exclusively composed of mirrors, creating an effectively repulsive boundary which halts self-assembly. Row 3 is characterized by this self-limiting behavior of single enantiomorph systems. Figure 6 shows the results for $c2mm$ (2*22) which produces dimers; $p31m$ (3*3) and $p4gm$ (4*2) result in trimers and tetramers, respectively (*cf.* ESI†). Here, $\langle N_n \rangle$ approaches the number of neighbors formed in a cluster and those clusters are perfectly formed, $\langle S_{A,B} \rangle \to 1$. A racemic mixture of polygons enables growth to occur along the mirrored edges, however, it creates ambiguity in terms of which enantiomorphs should combine around the rotation center. As before, local curvature ($\psi > 0°$) makes this unambiguous and leads to the best global assembly as S is the largest of these cases with $\langle S_{A,B} \rangle \to 1$, as in the single enantiomorph case. FD tiles characterized by this behavior are given in green in Fig. 2.

3.4 Row 2: Frieze (Smectic)

Enantiomorphically pure mixtures from row 2 assemble into what are characterized as "1D strings" in Fig. 5. FDs for these groups simultaneously have (1) a pair of 2-fold rotation centers and/or a pair of edges which are translated images of each other, while also having (2) all additional edges be either glides or mirrors. Effectively, this enables the system to assemble by allowing SDAs of the same chirality to match along edges via condition (1), while condition (2) inhibits growth in other directions. A pattern in two dimensions that is repetitive in only one of them is called a Frieze pattern. The FDs selected in row 2 of Fig. 2 are rectangles which satisfy these conditions. The mirror lines are indicated by black and magenta lines for $p2mg$ (22*), while the green and blue sinusoidal edges allow growth via sequential 2-fold rotation; the result is a $p2$ "dizzyhop" Frieze group whose orbifold symbol is 22∞.[34] Similarly, for $p1m1$ (**) growth is only possible by matching along the red edges of the quadrilateral FD in Fig. 2. The result is simple a repetition of translation, or a $p1$ ($\infty\infty$) "hop" Frieze group.[34] The same is true of the FD chosen for $p1g1$ (xx) in this work.

Figure 6 illustrates the observed self-assembly for $p1g1$. In an enantiomorphically pure system, 1D strings of SDAs assemble perfectly at first ($\langle S_{A,B} \rangle \to 1$) as shown by the blue curves; however, about halfway through the simulation shown, the number of neighbors rises sharply corresponding to a decline in the average pairwise score. This is a result of these strings aggregating along their mirror edge via the "single point defects" described in Fig. 5, in which only a single pair of beads can correctly align yielding an interaction energy of $U = -\varepsilon$. While the energetic benefit to a single pair of SDAs aggregating in this fashion is relatively small, the total energy scales with the number of SDAs interacting, *i.e.*, the length of the smaller of any two approaching strings such that $U_{tot} = -N_{smaller}\varepsilon$. There will always be some length, N_{min}, above which the total (favorable) interaction energy exceeds thermal energy ($|U_{tot}| > k_B T$) causing sufficiently long strings to randomly attach to another. As a result, these systems are better characterized as smectic since they result in ordered strings in one direction, but which are not necessarily aligned in the orthogonal direction. As before, a racemic mixture of undeformed, polygonal SDAs can assemble along edges, but form defects which tend to

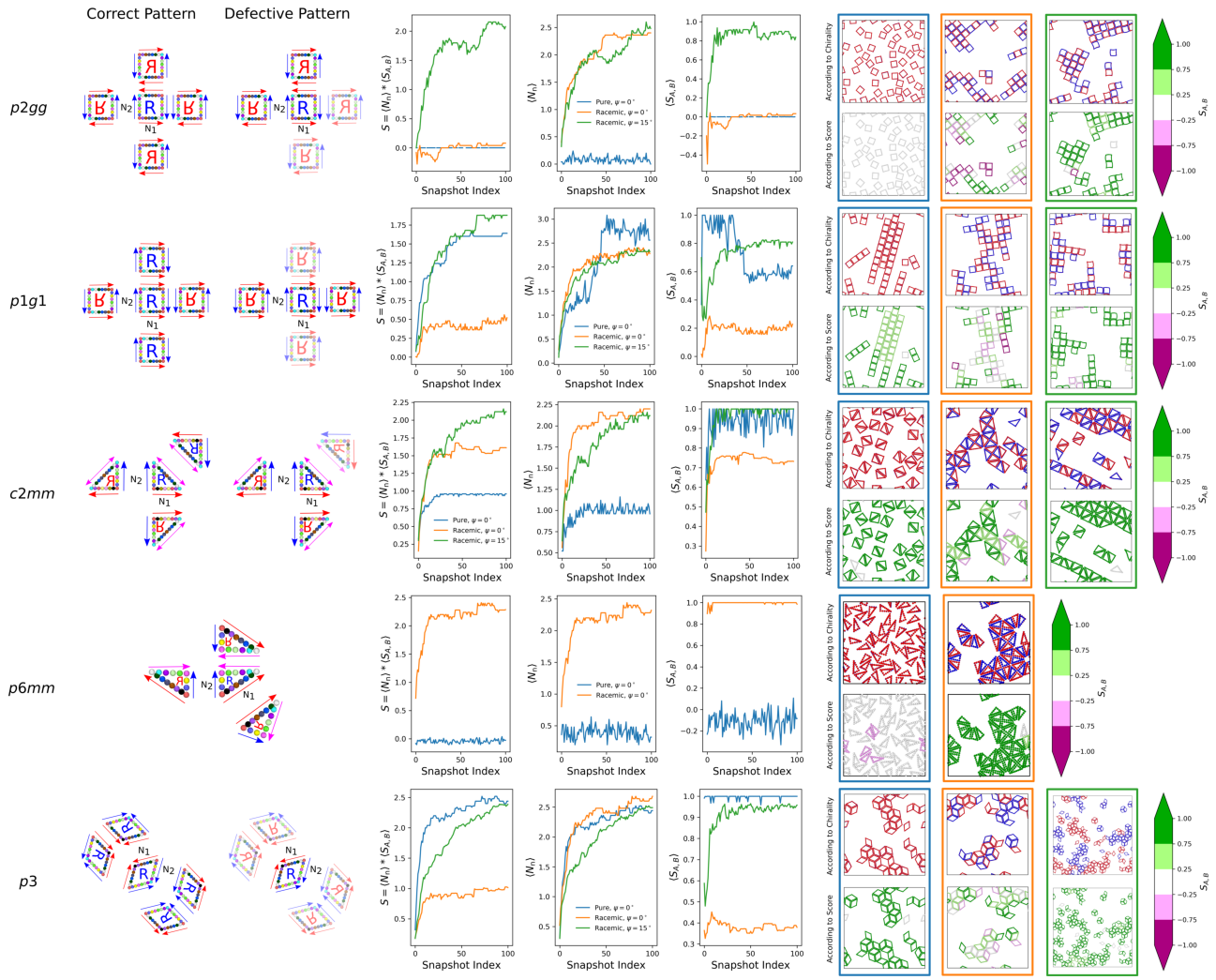

Fig. 6 Representative self-assembly characteristics for each row in Fig. 5. For each row, a group is selected and a cartoon of the undeformed rings illustrates the correct pattern for assembly, and an example defect due to inclusion of the wrong chirality. An asymmetric "R" motif is drawn as a guide to the eye, colored blue and red to indicate different ring chiralities (L *vs.* D). The first three graphs illustrate the global score, S, and its individual components for the three representative cases of: (1) a single chirality system of undeformed rings, (2) a racemic mixture of undeformed rings, and (3) a racemic mixture of deformed rings. Snapshots of the last frame in these simulations are shown at the right, outlined in the color corresponding to the score curves: blue, orange, and green for cases (1), (2), and (3), respectively. The upper snapshots are of the rings themselves colored according to chirality (red or blue, arbitrary), while the lower image is colored according to $S_{A,B}$ divided into 5 bins as illustrated by the colorbar at the right.

interrupt long range order since correct growth is now possible, but is not sufficiently specific, in two dimensions. Adding curvature along the edges penalizes these defects, adding the required specificity, which leads to optimal assembly in 2D (largest possible $\langle S \rangle$). All tiles that have this characteristic behavior are colored blue in Fig. 2.

While there is only 1 possible FD for $p1m1$, there are 4 possible for $p2mg$;[29,34,40] however, because of the parallel mirror symmetry lines in both groups, all possible FDs satisfy the conditions for 1D growth in an enantiomorphically pure system. In practice, some tiles form a bilayer instead of a monolayer of SDAs; for example, tile 15 for $p2mg$ or tile 4 for $p2gg$, as shown at the top of Fig. 2. The $p1g1$ (xx) group is characterized by parallel glide lines instead, which admits 4 topologically distinct FDs.[29,34,40] In 3 of these, the conditions above are satisfied, though there exists a fourth (tile 17) which behaves differently and is colored orange instead.

3.5 Row 1: Pluripotent (e[X]ceptions)

Although there are multiple different FDs for most groups, until this point all possible alternatives have carried the same defining characteristics that lead to the assembly behavior defining each row. For $p1g1$ (xx), described in the previous section with row 2, there are 4 topologically different tiles that can serve as the FD. For 3 out of the 4 possibilities, the conditions describing row 2 are satisfied; however, in tile 17 there are 2 pairs of edges related by glide operations, thus each can only align with an edge on the opposite enantiomorph. This inhibition of growth in an enantiomorphically pure case is what characterizes the kaleidoscopes in row 4 and thus it is colored as such in Fig. 2. While $p1g1$ (xx) has only 1 exception, there are two other groups which can adopt different behaviors based on one's choice of the FD tile.

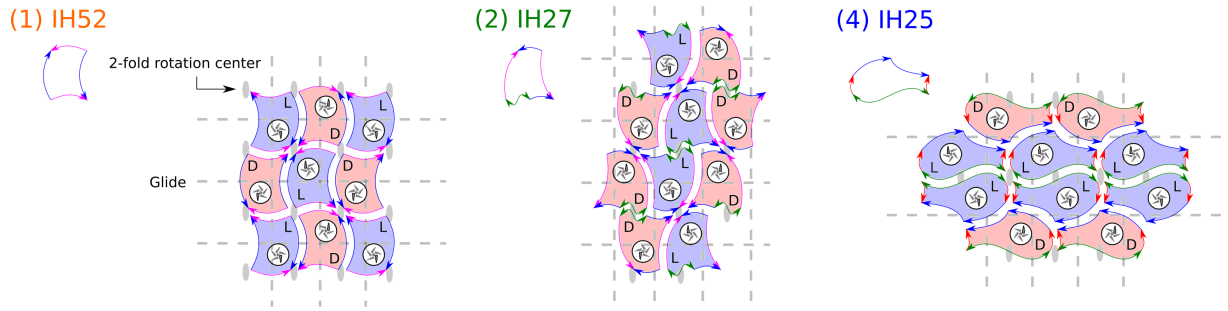

Fig. 7 Examples of different isohedral tiles that are fundamental domains for $p2gg$ (22x) as shown in Fig. 2. Symmetry operations for this group are indicated by dashed lines (glides) and ellipses (2-fold rotation centers). IH52 has 2 pairs of edges related by glide reflections and so each enantiomorph (L shown in blue, D in red) is surrounded by its opposite leading to assembly behavior akin to row 4. IH27 has an additional 2-fold rotation center allowing for pairs to form, surrounded by their opposite enantiomorph; this produces discrete dimers as in row 3. Finally, IH25 has assembly akin to row 2 since it is formed by rows of SDAs with the same chirality.

These groups are contained in the gray triangle in Fig. 5 and are outlined in Fig. 2.

These exceptions happen to correspond to all groups which contain a crosscap ($\times$) in their orbifold symbol. The mnemonic capitalization of "X" in this section's title may serve as a reminder for the reader. Note the choice of FDs for $p2gg$ (22x) and $c1m1$ (*x) selected here expose only mirror and glide edges, and thus exhibit self-assembly behavior characteristic of row 4 (kaleidoscopes, orange); however, these groups are not addressably complex and in the absence of edge curvature, which is not allowed in row 4 since all edges are mirrors there, defective assembly occurs. Figure 6 illustrates this confusion between glide and simple reflection, which results in some tiles being a 180° rotation of their correct orientation.

For $c1m1$ (*x) there are 3 topologically distinct FDs that can be selected. Tiles 9 and 10 behave as described and are reminiscent of row 4, whereas tile 11 is shown in blue in Fig. 2 and limits single enantiomorph systems to correct assembly in only one dimension by exposing a pair of edges that are translation images of each other (row 2). This results in a $p1$ Frieze pattern. The $p2gg$ (22x) group has 8 possible FDs, the largest of any group. Some expose a single 2-fold rotation center leading to assembly behavior found in row 3 (tiles 2 and 3), while others expose two centers and/or translate pairs leading to row 2 behavior (tiles 4–8), though now as a $p2$ Frieze pattern (*cf.* Fig. 7). When the mixture is racemic, and the SDA's edges are appropriately curved, they will assembly ideally as in all cases.

4 Discussion

To experimentally realize these designs, one must achieve three things: (1) control of patterning around the perimeter of the SDA, (2) control over its shape, including the creation of non-zero curvature along its edges, and (3) a way for the SDA to recruit or adsorb the object of interest in a stereospecific manner. There are a number of existing approaches that could be leveraged to achieve this control, perhaps chief among them is DNA-based nanotechnology.[14,51,52] DNA "tiles" designed using mathematical tiling theory and other insights have been successfully employed to assemble a wide range of periodic and aperiodic structures.[14,15,53–59] These SDAs may be regarded material "pixels"; in 3D, DNA-based frameworks have been successfully engineered for organizing nanoparticles using material "voxels" programmed by their inter-voxel bonds.[8] To date only a limited number of symmetries have been reported, though.

Other potential routes to experimental realization include peptidic nanostructures which have also been assembled into various symmetries[60,61] by controlling their interfacial properties[62] or by combining nanoparticles and polymers.[63,64] Tunable orthogonal reversible covalently (TORC) bonded systems may also enable realization of specific bonding patterns or chemical identities on an SDA.[65]

As for the curvature requirement, the construction of bent rods from DNA origami has already been demonstrated[66] and it is conceivable that these could be further assembled into SDAs using similar methods or, for example, by employing adsorbing nanoparticles to act as corners.[10,11,63,67,68] To achieve the final point, DNA "printing" or "stamping" promises high-fidelity functionalization of arbitrary, anisotropic objects,[69,70] and exquisite spatial control over particle functionalization has been demonstrated via other methods in numerous instances.[21,46,52,67,71–79] We note that this somewhat relaxes the immutability assumption initially asserted for the cargo being organized, though attaching "tethers" to particles is a mainstay of nanotechnology in terms of assembly methods.

Importantly, the favorable self-interaction of symmetrically identical sites would require that DNA sequences used along edges be self-complementary. In that case, the strands must be prevented from hybridizing with themselves instead of different partners. Linker mediated interactions[50,80–85] or oligonucleotide "staples"[86] may offer an alternative route which does not require this self-complementarity. Mirrored edges, in particular, require that an edge bind to an image of itself.

Most wallpaper groups contain reflection operations, including glides, and require both enantiomorphs to assemble, thus necessitating curvature to make rotation and reflection operations unambiguous based on their sequence. However, for gyration groups in row 5, if the system could be purified this would not be necessary. Regardless, we have assumed that practically these materials are expected to be prepared in a 3D environment where rotational diffusion will lead to racemization, meaning that edge

curvature is required even in this case. Another practical consideration of 3D synthesis is that the rings must be prevented from simply "stacking" on top of each other forming rouleaux. This can be achieved if the SDAs are constructed so that they only allow lateral interactions. In our 3-layer model [*cf.* Fig. 3(a)], the repulsive top and bottom layers would achieve this if not constrained to a planar interface; geometrically, this is similar in spirit to lipid rafts or "nanodiscs" constructed by encircling a lipid bilayer in a ring of amphipathic proteins.[87–89]

One important aspect of this design is that chiral enantiomorphs (mirror images) of the SDA ring are assumed to be identical rings that have been flipped out of the plane in which they are assembling. This means that tethered molecules or colloids on different enantiomorphs would also be flipped relative to each other, rather than being strictly reflected. Just like the SDA, which is truly a 3D object, if the cargo has mirror symmetry in the assembly plane, so that its "top" and "bottom" are identical, then this operation is identical to a reflection in the plane [*cf.* Fig. 3(a)]. If the cargo lacks this mirror symmetry, then the overall pattern will be different in the crystallographic sense. The SDA-driven organization is still regular and periodic, and may make no practical difference, but it bears consideration depending on the application.

In this work, we focused on the unambiguous case of directing the assembly of an asymmetric cargo, or motif (*cf.* 5-bladed pinwheel in Fig. 1). It is possible, however, for cargo with some symmetries (point preserving rotations or reflections) to induce some or all of those symmetries in the wallpaper group selected, creating an overall pattern with more symmetry that corresponds to a different group. In other words, if a colloid which is not entirely asymmetric is placed in a fortuitous location and orientation on an SDA tile used in this work, it is possible that from a crystallographic perspective: (1) the overall pattern no longer belongs to the symmetry group from which the SDA was derived, and (2) only a fraction of the colloid belongs to the true FD of the pattern. The conditions leading to this can be precisely enumerated with group theory and are available in references such as Ref.[29]. In general, these represent exceptions to the general case we have examined here. These exceptions cannot be disentangled from condition (2) which results in additional isohedral tiles, topologically distinct from the 46 used here, that can be used to assemble discrete cargo with internal symmetry. Such tiles require that the cargo has a certain symmetry and be carefully placed within the SDA at the correct location and orientation. Here we have focused on the cases which disregard this since we anticipate that most functional molecules or other nanoscale objects will not generally be highly symmetric, nor that they will need to be placed in such a particular fashion; the same is not necessarily true of, *e.g.*, patchy colloids. This is the subject of future work.

While such exceptions can be tedious to enumerate, there is one special case of particular importance for this work. Namely, for all SDAs derived from tiles associated with the groups indicated in black in Fig. 5 ($p1$, $p1m1$, $p1g1$, $c1m1$), the colloid being organized by them may never be an isotropic circle (or sphere).[29] The $p1$ group, in fact, carries the more restrictive condition that the colloid may never have any 2-fold rotational symmetry, nor be any supergroup of this (such as 4-fold, 6-fold, etc.) which includes the isotropic circle. Essentially, these objects add symmetry to the underlying pattern created by the assembling tiles, changing the symmetry unavoidably. This is of relevance, as there is a great deal of effort focused on using inverse design to engineer isotropic potentials to assemble arbitrary crystals.[41,90–94] This condition does not preclude the possibility of make a pattern belonging to one of these 4 wallpaper groups using isotropic particles, only that it is not possible to do so while simultaneously requiring that a single colloidal unit forms the fundamental domain.

Finally, we note that other taxonomies for 2D symmetry groups based on orbifolds have been developed. For example, Ref.[32] uses the topological connectedness, boundedness, and orientability of a group's orbifold to create categories. Such a mathematical organization has many merits, especially when unifying symmetry groups to include non-Euclidean spaces; by contrast, our taxonomy is based on characteristic differences in self-assembly occurring in the Euclidean plane. These are straightforward to rationalize based on the orbifold symbol, though tiles from groups with at least one topological crosscap require a more careful examination of the pattern of the FD's edges. Still, all possible tiles for each group are derivable from its orbifold.[34] We anticipate that our taxonomy may have more practical utility than a purely mathematical catalog. For example, all kaleidoscopes in row 4 are also categorized as a single class in Ref.[32], however, therein $p2mg$ (22*) from row 2 is combined with those in row 3 since they are simply connected, bounded, and orientable. Yet, it is clear that having a pair of rotation centers enables $p2mg$ to grow without bound in 1D for single enantiomorph mixtures, while the others exhibit fully self-limited growth since they contain only a single center. As another example, the $p1$ group is also excluded from row 5 and categorized separately in Ref.[32], while we consider it together with the palindromic groups since it can undergo chiral phase separation.

5 Conclusions

We have used symmetry to derive self-assembling structure directing agents for templating arbitrary colloidal objects into infinitely repeating patterns at a planar interface. We further developed a taxonomy based on their self-assembly characteristics and illustrated how these characteristics are explicitly reflected by their orbifold symbol. Our design strategy is based on a symmetry group's fundamental domain, which is free to contain any object of any (a)symmetry, since the crystal's symmetry is encoded at the domain's boundary not in its interior. Thus, it is a natural structure to base the SDA on, which effectively reduces this design to a tiling problem.

We assumed that such systems will be naturally racemic due to rotational diffusion of the SDAs during manufacturing; in fact, most groups contain reflection operations and therefore require a racemic mixture to assemble, regardless. In this case, non-zero curvature of the tile's edges is required to unambiguously represent the symmetry operation encoded at an edge and prevent defective self-assembly. The result is essentially defect-free assembly of the SDA into the desired wallpaper group.

Such an SDA may be used to encompass a single colloid, which may itself be a pre-assembled set of more than one object; however, it may be desirable to place less than one, or a non-integer number of colloidal units, into a fundamental domain to create a desired crystal. The approach described here does not enable this, as crossing a boundary imposes symmetry on the colloid itself, implying the object could not truly be "arbitrary"; however, adaptations to accommodate such symmetries are the subject of future work.

Overall, we found 5 different characteristic self-assembly behaviors based largely on insights from the behavior of single enantiomorph systems. This includes systems which naturally undergo chiral phase separation (row 5), are addressably complex (row 4), exhibit self-limiting growth (row 3), form one dimensional rods akin to smectic phases (row 2), and ones for which different fundamental domain tiles can induce different characteristic behaviors, but still result in the same final symmetry. Therefore, by choosing a certain tile and controlling the chirality of the mixture, it is possible to control the self-assembly pathway the system adopts.

Conflicts of interest

There are no conflicts to declare.

Acknowledgements

Contribution of the National Institute of Standards and Technology, not subject to US Copyright.

Notes and references

1 V. N. Manoharan, *Science*, 2015, **349**, 1253751.

2 M. A. Boles, M. Engel and D. V. Talapin, *Chemical Reviews*, 2016, **116**, 11220–11289.

3 K. R. Phillips, G. T. England, S. Sunny, E. Shirman, T. Shirman, N. Vogel and J. Aizenberg, *Chemical Society Reviews*, 2016, **45**, 281–322.

4 K. Ariga, M. Nishikawa, T. Mori, J. Takeya, L. K. Shrestha and J. P. Hill, *Science and Technology of Advanced Materials*, 2019, **20**, 51–95.

5 M. He, J. P. Gales, É. Ducrot, Z. Gong, G.-R. Yi, S. Sacanna and D. J. Pine, *Nature*, 2020, **585**, 524–529.

6 W. C. Poon, A. T. Brown, S. O. Direito, D. J. Hodgson, L. Le Nagard, A. Lips, C. E. MacPhee, D. Marenduzzo, J. R. Royer, A. F. Silva *et al.*, *Soft Matter*, 2020, **16**, 8310–8324.

7 N. Vogel, M. Retsch, C.-A. Fustin, A. del Campo and U. Jonas, *Chemical Reviews*, 2015, **115**, 6265–6311.

8 Y. Tian, J. R. Lhermitte, L. Bai, T. Vo, H. L. Xin, H. Li, R. Li, M. Fukuto, K. G. Yager, J. S. Kahn, Y. Xiong, B. Minevich, S. K. Kumar and O. Gang, *Nature Materials*, 2020, **19**, 789–796.

9 J. D. Halverson and A. V. Tkachenko, *The Journal of Chemical Physics*, 2017, **147**, 141103.

10 W. Liu, J. Halverson, Y. Tian, A. Tkachenko and O. Gang, *Nature Chemistry*, 2016, **8**, 867–873.

11 Y. Tian, Y. Zhang, T. Wang, H. L. Xin, H. Li and O. Gang, *Nature Materials*, 2016, **15**, 654–661.

12 W. Wang, S. Chen, B. An, K. Huang, T. Bai, M. Xu, G. Bellot, Y. Ke, Y. Xiang and B. Wei, *Nature Communications*, 2019, **10**, 1–8.

13 E. Winfree, *American Mathematical Society*, 1996.

14 E. Winfree, F. Liu, L. A. Wenzler and N. C. Seeman, *Nature*, 1998, **394**, 539–544.

15 P. W. Rothemund, N. Papadakis and E. Winfree, *PLoS Biol*, 2004, **2**, e424.

16 E. Eteshola and D. Leckband, *Sensors and Actuators B: Chemical*, 2001, **72**, 129–133.

17 R. M. Lequin, *Clinical Chemistry*, 2005, **51**, 2415–2418.

18 D. B. Bush and T. A. Knotts IV, *The Journal of Chemical Physics*, 2015, **143**, 061101.

19 P. Praveschotinunt, A. M. Duraj-Thatte, I. Gelfat, F. Bahl, D. B. Chou and N. S. Joshi, *Nature Communications*, 2019, **10**, 1–14.

20 J. Su, M. O. De La Cruz and H. Guo, *Physical Review E*, 2012, **85**, 011504.

21 X. Lin, J. C. Lu, Y. Shao, Y. Y. Zhang, X. Wu, J. B. Pan, L. Gao, S. Y. Zhu, K. Qian, Y. F. Zhang, D. L. Bao, L. F. Li, Y. Q. Wang, Z. L. Liu, J. T. Sun, T. Lei, C. Liu, J. O. Wang, K. Ibrahim, D. N. Leonard, W. Zhou, H. M. Guo, Y. L. Wang, S. X. Du, S. T. Pantelides and H.-J. Gao, *Nature Materials*, 2017, **16**, 717–721.

22 M. Witman, S. Ling, P. Boyd, S. Barthel, M. Haranczyk, B. Slater and B. Smit, *ACS Central Science*, 2018, **4**, 235–245.

23 J. I. Monroe and M. S. Shell, *Proceedings of the National Academy of Sciences*, 2018, **115**, 8093–8098.

24 S. T. Henriques, H. Peacock, A. H. Benfield, C. K. Wang and D. J. Craik, *Journal of the American Chemical Society*, 2019, **141**, 20460–20469.

25 O. I. Wilner, Y. Weizmann, R. Gill, O. Lioubashevski, R. Freeman and I. Willner, *Nature Nanotechnology*, 2009, **4**, 249–254.

26 G. Prieto, H. Tüysüz, N. Duyckaerts, J. Knossalla, G.-H. Wang and F. Schuüth, *Chemical Reviews*, 2016, **116**, 14056–14119.

27 N. Vogel, S. Utech, G. T. England, T. Shirman, K. R. Phillips, N. Koay, I. B. Burgess, M. Kolle, D. A. Weitz and J. Aizenberg, *Proceedings of the National Academy of Sciences*, 2015, **112**, 10845–10850.

28 S.-H. Kim, S. Magkiriadou, D. K. Rhee, D. S. Lee, P. J. Yoo, V. N. Manoharan and G.-R. Yi, *ACS Applied Materials & Interfaces*, 2017, **9**, 24155–24160.

29 B. Grünbaum and G. C. Shepherd, *Tilings and Patterns*, 2016.

30 W. P. Thurston, *The geometry and topology of three-manifolds*, Princeton University; Princeton, NJ, 1979.

31 J. Conway, *London Mathematical Society Lecture Note Series 165*, Cambridge University Press, Cambridge, 1992, pp. 438–447.

32 S. Hyde, S. Ramsden and V. Robins, *Acta Crystallographica Section A: Foundations and Advances*, 2014, **70**, 319–337.

33 *International Tables for Crystallography Volume A: Space-group Symmetry*, International Union of Crystallography, 1983.

34 J. H. Conway, H. Burgiel and C. Goodman-Strauss, *The symmetries of things*, CRC Press, 2016.

35 A. M. Macbeath, *Canadian Journal of Mathematics*, 1967, **19**, 1192–1205.

36 J. H. Conway and D. H. Huson, *Structural Chemistry*, 2002, **13**, 247–257.

37 C. K. Johnson, M. N. Burnett and W. D. Dunbar, *Crystallographic Computing*, 1996, **7**, 1–25.

38 B. N. Delone, *Izvestiya Rossiiskoi Akademii Nauk. Seriya Matematicheskaya*, 1959, **23**, 365–386.

39 J. H. Conway, O. Delgado Friedrichs, D. H. Huson and W. Thurston, *Contributions to Algebra and Geometry*, 2001, **42**, 475–507.

40 H. Heesch and O. Kienzle, *Flächenschluß. Buchreihe Wissenschaftliche Normung*, 1963.

41 N. A. Mahynski, E. Pretti, V. K. Shen and J. Mittal, *Nature Communications*, 2019, **10**, 2028.

42 E. Pretti, V. K. Shen, J. Mittal and N. A. Mahynski, *The Journal of Physical Chemistry A*, 2020, **124**, 3276–3285.

43 S. Plimpton, *Journal of Computational Physics*, 1995, **117**, 1–19.

44 W. M. Jacobs, A. Reinhardt and D. Frenkel, *Proceedings of the National Academy of Sciences*, 2015, **112**, 6313–6318.

45 W. M. Jacobs and D. Frenkel, *Journal of the American Chemical Society*, 2016, **138**, 2457–2467.

46 M. R. Jones, N. C. Seeman and C. A. Mirkin, *Science*, 2015, **347**, 1260901.

47 W. B. Rogers, W. M. Shih and V. N. Manoharan, *Nature Reviews Materials*, 2016, **1**, 1–14.

48 J. Madge and M. A. Miller, *Soft matter*, 2017, **13**, 7780–7792.

49 S. N. Fejer, R. G. Mantell and D. J. Wales, *Molecular Physics*, 2018, **116**, 2954–2964.

50 W. B. Rogers, *The Journal of Chemical Physics*, 2020, **153**, 124901.

51 N. C. Seeman, *Angewandte Chemie International Edition*, 1998, **37**, 3220–3238.

52 P. W. K. Rothemund, *Nature*, 2006, **440**, 297–302.

53 A. Chworos, I. Severcan, A. Y. Koyfman, P. Weinkam, E. Oroudjev, H. G. Hansma and L. Jaeger, *Science*, 2004, **306**, 2068–2072.

54 S. H. Park, C. Pistol, S. J. Ahn, J. H. Reif, A. R. Lebeck, C. Dwyer and T. H. LaBean, *Angewandte Chemie*, 2006, **118**, 749–753.

55 C. Lin, Y. Liu, S. Rinker and H. Yan, *ChemPhysChem*, 2006, **7**, 1641–1647.

56 X. Ye, J. Chen, M. Engel, J. A. Millan, W. Li, L. Qi, G. Xing, J. E. Collins, C. R. Kagan, J. Li *et al.*, *Nature Chemistry*, 2013, **5**, 466–473.

57 J. A. Millan, D. Ortiz, G. Van Anders and S. C. Glotzer, *ACS Nano*, 2014, **8**, 2918–2928.

58 F. Zhang, S. Jiang, W. Li, A. Hunt, Y. Liu and H. Yan, *Angewandte Chemie International Edition*, 2016, **55**, 8860–8863.

59 C. Karner, C. Dellago and E. Bianchi, *Nano Letters*, 2019, **19**, 7806–7815.

60 J. E. Padilla, C. Colovos and T. O. Yeates, *Proceedings of the National Academy of Sciences*, 2001, **98**, 2217–2221.

61 H. Yan, S. H. Park, G. Finkelstein, J. H. Reif and T. H. LaBean, *Science*, 2003, **301**, 1882–1884.

62 S. Gonen, F. DiMaio, T. Gonen and D. Baker, *Science*, 2015, **348**, 1365–1368.

63 W. Bai, C. J. Sargent, J.-M. Choi, R. V. Pappu and F. Zhang, *Nature Communications*, 2019, **10**, 1–10.

64 T. Sawada and M. Fujita, *Chem*, 2020, **6**, 1861–1876.

65 J. F. Reuther, S. D. Dahlhauser and E. V. Anslyn, *Angewandte Chemie International Edition*, 2019, **58**, 74–85.

66 H. Dietz, S. M. Douglas and W. M. Shih, *Science*, 2009, **325**, 725–730.

67 Y. Tian, T. Wang, W. Liu, H. L. Xin, H. Li, Y. Ke, W. M. Shih and O. Gang, *Nature Nanotechnology*, 2015, **10**, 637–644.

68 W. Liu, N. A. Mahynski, O. Gang, A. Z. Panagiotopoulos and S. K. Kumar, *ACS Nano*, 2017, **11**, 4950–4959.

69 Y. Xiong, S. Yang, Y. Tian, A. Michelson, S. Xiang, H. Xin and O. Gang, *ACS Nano*, 2020, **14**, 6823–6833.

70 F. J. Rizzuto, T. Trinh and H. F. Sleiman, *Chem*, 2020, **6**, 1560–1574.

71 J. K. Kummerfeld, T. S. Hudson and P. Harrowell, *The Journal of Physical Chemistry Letters B*, 2008, **112**, 10773–10776.

72 Q. Chen, S. C. Bae and S. Granick, *Nature*, 2011, **469**, 381–384.

73 R. J. Macfarlane, B. Lee, M. R. Jones, N. Harris, G. C. Schatz and C. A. Mirkin, *Science*, 2011, **334**, 204–208.

74 Y. Wang, Y. Wang, D. R. Breed, V. N. Manoharan, L. Feng, A. D. Hollingsworth, M. Weck and D. J. Pine, *Nature*, 2012, **491**, 51–55.

75 B. G. van Ravensteijn, M. Kamp, A. van Blaaderen and W. K. Kegel, *Chemistry of Materials*, 2013, **25**, 4348–4353.

76 E. Auyeung, T. I. N. G. Li, A. J. Senesi, A. L. Schmucker, B. C. Pals, M. Olvera de la Cruz and C. A. Mirkin, *Nature*, 2014, **505**, 73–77.

77 M. N. O'Brien, M. R. Jones and C. A. Mirkin, *Proceedings of the National Academy of Science*, 2016, **113**, 11717–11725.

78 N. Patra and A. V. Tkachenko, *Physical Review E*, 2017, **96**, 022601.

79 L. Peng, Z. Fang, J. Li, L. Wang, A. M. Bruck, Y. Zhu, Y. Zhang, K. J. Takeuchi, A. C. Marschilok, E. A. Stach, E. S. Takeuchi and G. Yu, *ACS Nano*, 2018, **12**, 820–828.

80 J. Zheng, P. E. Constantinou, C. Micheel, A. P. Alivisatos, R. A. Kiehl and N. C. Seeman, *Nano Letters*, 2006, **6**, 1502–1504.

81 J. T. McGinley, Y. Wang, I. C. Jenkins, T. Sinno and J. C. Crocker, *ACS Nano*, 2015, **9**, 10817–10825.

82 S. Borsley and E. R. Kay, *Chemical Communications*, 2016, **52**, 9117–9120.

83 B. A. Lindquist, R. B. Jadrich, D. J. Milliron and T. M. Truskett, *The Journal of Chemical Physics*, 2016, **145**, 074906.

84 M. P. Howard, R. B. Jadrich, B. A. Lindquist, F. Khabaz, R. T. Bonnecaze, D. J. Milliron and T. M. Truskett, *The Journal of Chemical Physics*, 2019, **151**, 124901.

85 M. Girard, S. Wang, J. S. Du, A. Das, Z. Huang, V. P. Dravid, B. Lee, C. A. Mirkin and M. O. de la Cruz, *Science*, 2019, **364**,

1174–1178.

86 F. Praetorius and H. Dietz, *Science*, 2017, **355**, eaam5488.

87 I. G. Denisov, Y. V. Grinkova, A. A. Lazarides and S. G. Sligar, *Journal of the American Chemical Society*, 2004, **126**, 3477–3487.

88 M. Wadsäter, S. Maric, J. B. Simonsen, K. Mortensen and M. Cardenas, *Soft Matter*, 2013, **9**, 2329–2337.

89 P. A. Beales, N. Geerts, K. K. Inampudi, H. Shigematsu, C. J. Wilson and T. K. Vanderlick, *Journal of the American Chemical Society*, 2013, **135**, 3335–3338.

90 A. Jain, J. R. Errington and T. M. Truskett, *Physical Review X*, 2014, **4**, 031049.

91 C. S. Adorf, J. Antonaglia, J. Dshemuchadse and S. C. Glotzer, *The Journal of Chemical Physics*, 2018, **149**, 204102.

92 D. Banerjee, B. A. Lindquist, R. B. Jadrich and T. M. Truskett, *The Journal of Chemical Physics*, 2019, **150**, 124903.

93 N. A. Mahynski, R. Mao, E. Pretti, V. K. Shen and J. Mittal, *Soft Matter*, 2020, **16**, 3187–3194.

94 J. Dshemuchadse, P. F. Damasceno, C. L. Phillips, M. Engel and S. C. Glotzer, *Proceedings of the National Academy of Sciences*, 2021, **118**, e2024034118.